Catalysis Today 321–322 (2019) 113–119

Contents lists available at ScienceDirect

Catalysis Today

journal homepage: www.elsevier.com/locate/cattod

Photocatalytic H_2 production over inverse opal TiO_2 catalysts

Roberto Fiorenza[a,*], Marianna Bellardita[b], Salvatore Scirè[a], Leonardo Palmisano[b]

[a] Dip. Scienze Chimiche, Università di Catania, Viale A. Doria 6, 95125 Catania, Italy
[b] DEIM, Università di Palermo, Viale delle Scienze, 90128 Palermo, Italy

ARTICLE INFO

Keywords:
Photocatalysis
Titanium dioxide
Water splitting
Photonic effect
Porous structures

ABSTRACT

The influence of $BiVO_4$ and CuO on the chemico-physical properties of TiO_2-based systems is reported. The performances of these systems were investigated in the photocatalytic H_2 production both under UV and solar light irradiation. The characterization data pointed out that the obtained TiO_2 samples have highly porous inverse opal structures with interconnected macropores. Inverse opal TiO_2 exhibited higher activity in the H_2 production than the commercial TiO_2 due to the peculiar porosity that allows photons to enter inside the photocatalyst. A further improvement in terms of photoactivity was verified by addition of increasing amounts of $BiVO_4$. On the contrary a small CuO content was found to be the optimal one for the inverse opal TiO_2-CuO composites. In fact, due to surface segregation effects, a higher amount of CuO can partially keep the light radiation away from the TiO_2 surface active sites, thus decreasing drastically the absorption of photons. The combination of the benefits of the highly ordered porous TiO_2 structure and the presence of $BiVO_4$ or small amounts of CuO can represent a promising strategy towards efficient photocatalytic H_2 production.

1. Introduction

The environmental harms and the energy crisis are among the main concerns of modern society. The progressive depletion of fossil fuel reserves and the environmental pollution caused by the combustion of them make H_2 more attractive as clean, storable and environmentally friendly fuel [1,2]. However, being H_2 an energy carrier, it is necessary to develop sustainable and green methods for its production. Since Fujishima and Honda reported the photoelectrochemical evolution of H_2 on the TiO_2 electrode in 1972 [3], the photoactivity of TiO_2-based materials was intensively investigated both for the photocatalytic water splitting and degradation of toxic organics. Titanium dioxide exhibits some advantages due to its stability, low cost, and no toxicity [4,5]. To improve the photocatalytic efficiency of TiO_2, much effort has been made to modify the size, the morphology, the electronic structure and the preparation method. In particular, mesoporous structures have been studied due to their large accessible surface area and well defined uniform pore size and intrinsic connectivity, which favour an efficient charge carrier transfer and mass flow of the reactants [6,7]. In this contest, three-dimensional inverse opal structures prepared by template strategy were recently investigated as a promising class of photocatalysts with peculiar structure and macro-mesoporosity [8–10]. In these materials the particular porous backbone acts in fact as a photon trap, taking advantage also of the scattering effects [11,12]. An important issue for active materials in the photocatalytic reactions is, in fact, the light absorption property which is strongly correlated with the conversion efficiency of photons to electrons.

Another approach to enhance the photoactivity is the combination of TiO_2 with noble metals (Pt, Ag or Au) or other oxides [13–15]. Non-noble metals co-catalysts such as cobalt or copper have also shown good photocatalytic performance in the water splitting reaction [16–18] with the advantage of lower cost compared to noble metals. In particular, several investigations showed that the TiO_2-CuO composites are efficient photocatalysts for water splitting to produce H_2 [19,20]. The presence of CuO provides active sites for H_2 evolution enhancing also the electron-hole separation.

In this contest, also $BiVO_4$ is an attractive material for solar water splitting due to its small band gap (2.4 eV) which enables a wide absorption in the portion of the visible spectrum [21,22]. The good stability and the suitable valence band energy position to oxidize water are, in addition, key features either on its own or coupled with TiO_2 [23,24]. Furthermore, the combination of a highly ordered three dimensional macroporous titania (3DOM TiO_2) with $BiVO_4$ has achieved good results in the photodegredation of Rhodamine B under visible light irradiation [25].

On these bases, we studied the combination of structural (synthesis of inverse opal TiO_2 with a highly ordered porous framework) and chemical modifications of TiO_2 (addition of different amounts of CuO and $BiVO_4$ to the inverse opal TiO_2) with the aim to investigate how these changes can influence the H_2 production both under UV and solar

* Corresponding author.
E-mail address: rfiorenza@unict.it (R. Fiorenza).

https://doi.org/10.1016/j.cattod.2017.12.011
Received 29 June 2017; Received in revised form 12 October 2017; Accepted 9 December 2017
Available online 13 December 2017
0920-5861/

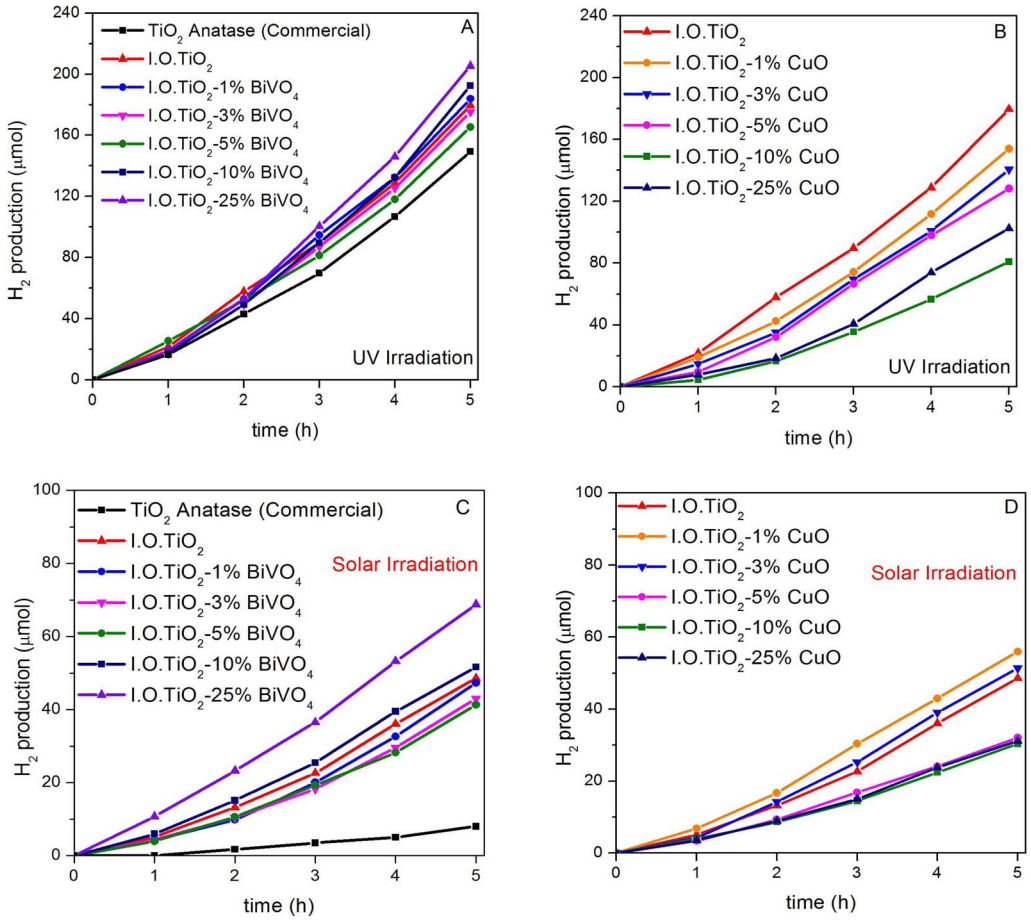

Fig. 1. Photocatalytic H_2 production at 30 °C: (A) Inverse Opal TiO_2-$BiVO_4$ and (B) Inverse Opal TiO_2-CuO composites under UV irradiation; (C) Inverse Opal TiO_2-$BiVO_4$ and (D) Inverse Opal TiO_2-CuO under solar light irradiation. (For interpretation of the references to colour in this figure text, the reader is referred to the web version of this article.)

light irradiation. From a practical point of view the solar water splitting is a promising strategy to produce H_2 without using fossil fuel playing a key role towards a sustainable hydrogen-based energy economy.

2. Experimental

2.1. Catalyst preparation

Inverse opal (I.O.) TiO_2 was synthesized via a templating strategy using polystyrene (PS) spheres, obtained by free-surfactant emulsion polymerization, according to the method previously reported in the literature [8,9,25]. Briefly, after the formation of the PS spheres the following steps consisted of an infiltration procedure with a solution of titanium isopropoxide, drying for 24 h and calcining at 550 °C for 12 h (heating ramp of 2 °C/min) leading to the formation of the inverse opal TiO_2 structure through the removal of the PS template.

The I.O. TiO_2-CuO composites were prepared by adding a proper amount of the metal salt precursor (copper(II) chloride) to the titanium isopropoxide-sol used for the infiltration.

The I.O TiO_2-$BiVO_4$ composites were prepared by the hydrothermal method by mixing stoichiometric amounts of $Bi(NO_3)_3{\cdot}5H_2O$ and NH_4VO_3 with an ethylene glycol-water solution, stirring until the obtainment of a clear solution [25,26]. Subsequently, after the addition of the I.O. TiO_2 powder, the mixture was sonicated for 15 min, stirred for 1 h and heated at 160 °C for 24 h inside a Teflon autoclave. Washing with distilled water, drying at 100 °C for 24 h and calcination at 300 °C for 3 h (ramp of 2 °C/min) were the final steps to synthesize the inverse opal TiO_2-$BiVO_4$ systems.

All TiO_2-composites were prepared with different nominal concentrations of copper oxide and bismuth vanadate (from 1 to 25% weight percentages).

A commercial sample of TiO_2 anatase (Sigma Aldrich prod. Nos. 637254, surface area 42 m^2/g) was used for the photocatalytic activity comparisons.

2.2. Catalyst characterization

The structure and the morphology of the samples were evaluated by scanning electron microscopy (SEM) using a Jeol JSM-7500F instrument, and by transmission electron microscopy (TEM) using a Jeol JEM 2100F operating at 200 kV.

The X-ray powder diffraction (XRD) measurements were carried out with a PANalytical X'pertPro X-ray diffractometer using a Cu Kα radiation. The JCPDS Data File was utilized to compare the detected diffraction peaks of the samples.

The BET surface area of the composites were estimated by the nitrogen adsorption-desorption measurements with a Micromeritics Tristar 3000. Samples were outgassed at 120 °C overnight before the measurements.

The surface properties were investigated with a K-Alpha™ + X-ray photoelectron spectrometer. The C (1s) peak at 285.8 eV (coming from the adventitious carbon) was used as reference for the X-ray photoelectron spectroscopy (XPS) analyses.

Ultraviolet-Visible-Diffuse Reflectance Spectroscopy (UV–Vis DRS) was performed by Perkin Elmer Lambda 35 UV–vis spectrometer, and $BaSO_4$ was used as the reference.

2.3. Photocatalytic activity experiments

Hydrogen generation by photocatalytic reforming of aqueous ethanol solution was performed in a home-made Pyrex jacketed reactor thermostated at 30 °C. The evolution of H_2 was quantified by analyzing

the effluent gases with an online gas chromatograph equipped with a packed column (Carboxen 1000) and thermal conductivity detector using Argon as carrier gas. Specifically, the catalyst (25 mg) was placed inside the photo-reactor with 45 mL of deionized water and 5 mL of ethanol used as sacrificial agent, under stirring. The suspension was purged with an argon flow for at least 1 h before irradiation in order to remove dissolved air. Then it was irradiated for 5 h by using a UV 100 W Hg lamp (Blak-Ray B 100A, 365 nm) or a special lamp designed for sunlight simulation (Osram Ultra Vitalux 300 W).

3. Results and discussion

Fig. 1 shows H_2 evolution under UV and solar light irradiation in the presence of the investigated TiO_2 based systems. Under UV irradiation the bare I.O. TiO_2 (red line) showed a higher H_2 production compared to commercial TiO_2 anatase (black curve) (Fig. 1A–B). The presence of $BiVO_4$ (Fig. 1A) led to a moderate increase of H_2 production, which was more relevant for the samples with the highest amount (I.O. TiO_2-10% $BiVO_4$ and I.O. TiO_2-25%$BiVO_4$). On the contrary the addition of CuO (Fig. 1B) had a negative effect on the performance, even at a low copper amount.

Under solar light irradiation (Fig. 1C–D) the I.O. TiO_2 exhibited a much higher activity (about 5 times) compared to commercial TiO_2. Also in this case concentrations of $BiVO_4$ higher than 10 wt.% resulted in a further increase of the hydrogen production, with the I.O. TiO_2-25%$BiVO_4$ sample exhibiting the best performance (Fig. 1C violet line). On the contrary for the I.O. TiO_2-CuO composites (Fig. 1D) only the samples with small amounts of CuO (1–3 wt.%) had a better activity with respect to I.O. TiO_2. For all the samples the amount of H_2 produced under solar light irradiation was smaller than that found under UV irradiation. This finding can be explained by considering the values of band-gap energy of the TiO_2-based catalysts which are similar to that of the anatase bare TiO_2 (Table 1).

The higher photoactivity of I.O. TiO_2 compared to commercial TiO_2 anatase cannot be ascribed to a different TiO_2 phase. In fact, I.O. TiO_2 also adopts the anatase phase, as shown by XRD reported in Fig. 2 (signals at 2θ = 25.3°, 37.8°, 48.0°, 54.0° and 55.1° [27,28]). SEM and TEM images (Fig. 3) showed an ordered macroporous structure of I.O. TiO_2 with interconnections between the pores. Single porous domains are present inside the material, in agreement with the morphology of other inverse opals prepared with the template method [8,9,25]. This macroporosity can be claimed to explain the increased photoactivity, as it can favour the mass transfer and consequently the reduction of H^+ ions on the surface of TiO_2 by the photogenerated electrons. In addition, the ordered network can increase the optical path length of the incident light radiation caused by the multiple reflection inside the macroporous structure [29,30], generating at the end, more electron-hole pairs to split water. Notably, no substantial changes in the inverse opal TiO_2 morphology was observed in the presence of CuO or $BiVO_4$ (Fig. 4).

Table 1
Crystallite size (calculated by Scherrer equation), BET Surface area (S_{BET}) and Band-gap energy (E_g) for the investigated I.O. TiO_2 samples.

Catalysts	Crystallite size (nm)	S_{BET} ($m^2\,g^{-1}$)	E_g (eV)
I.O.-TiO_2	25.4	28.0	3.23
TiO_2-1%$BiVO_4$	25.1	28.3	3.19
TiO_2-3%$BiVO_4$	25.6	30.3	3.18
TiO_2-5%$BiVO_4$	26.2	29.7	3.17
TiO_2-10%$BiVO_4$	28.1	28.1	3.19
TiO_2-25%$BiVO_4$	29.3	27.3	3.17
TiO_2-1%CuO	22.8	32.7	3.25
TiO_2-3%CuO	21.9	31.4	3.19
TiO_2-5%CuO	20.0	33.0	3.16 2.04[a]
TiO_2-10%CuO	24.2	28.2	3.18 2.10[a]
TiO_2-25%CuO	25.6	29.5	3.14 2.06[a]

[a] Midgap value.

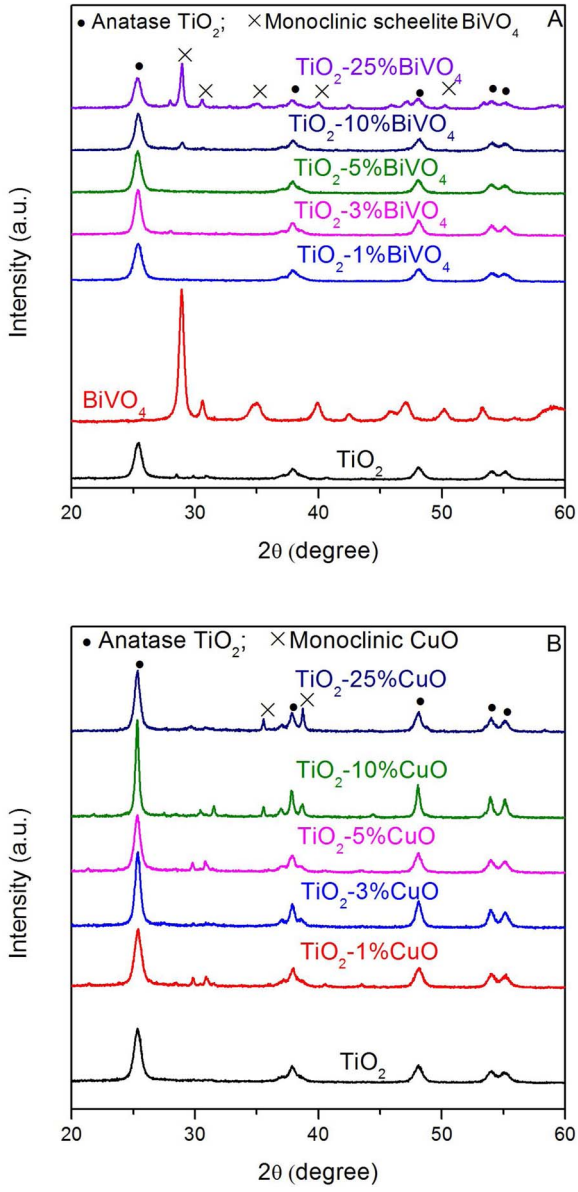

Fig. 2. XRD patterns of Inverse Opal TiO_2-$BiVO_4$ (A) and Inverse Opal TiO_2-CuO (B) systems.

The presence of I.O. TiO_2-CuO and I.O. TiO_2-$BiVO_4$ heterojunctions can be noticed in Fig. 4A and C, respectively. This finding was confirmed by determining the different lattice fringes of (101) TiO_2 (d = 0.35 nm), (200) CuO (d = 0.23 nm) and (130) $BiVO_4$ (d = 0.31 nm) [25,31]. Moreover Fig. 4B and D indicated that the porous structure of the I.O. TiO_2 was maintained in the composite systems.

To better understand the photocatalytic activity trend and the changes in the chemico-physical properties of the inverse opal TiO_2, due to the presence of $BiVO_4$ or CuO, the structural, optical and surface properties of the composites were evaluated by various techniques (XRD, surface area determination, UV–vis DRS and XPS).

The XRD patterns of I.O. TiO_2-$BiVO_4$ (Fig. 2A) show that only the samples with the 10 and 25 wt.% of $BiVO_4$ display both signals of TiO_2 (anatase) and $BiVO_4$ (monoclinic scheelite [32,33]). Similarly, also for the I.O. TiO_2-CuO series (Fig. 2B) the catalysts with a high amount of

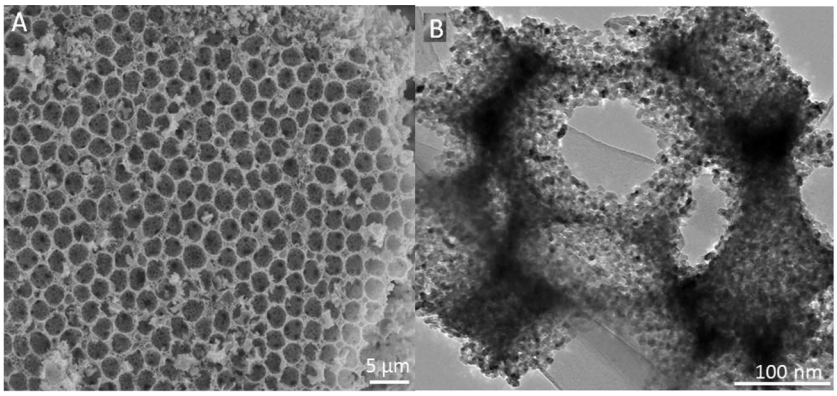

Fig. 3. SEM (A) and TEM (B) images of Inverse Opal TiO_2 sample.

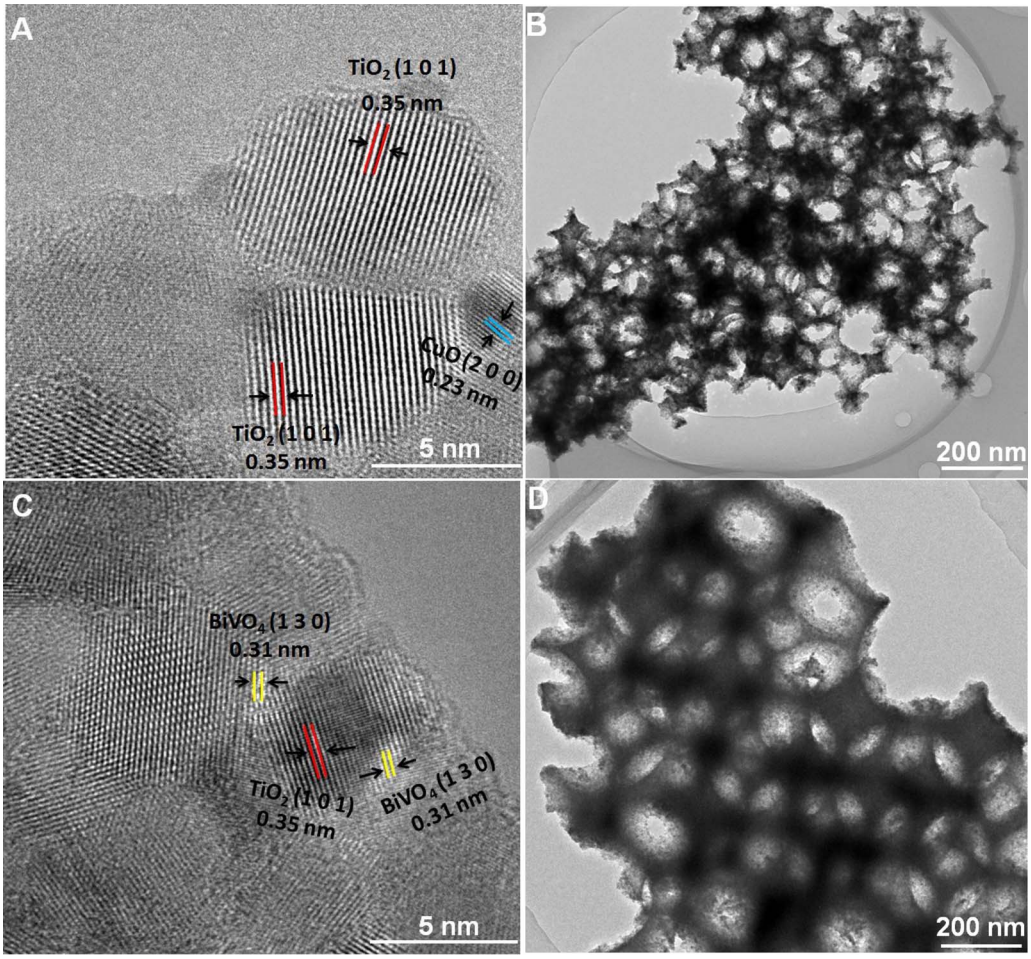

Fig. 4. TEM images of Inverse Opal TiO_2-3% CuO (A, B) and Inverse Opal TiO_2-10% $BiVO_4$ (C, D) samples.

copper oxide (I.O. TiO_2-10%CuO and I.O. TiO_2-25%CuO) exhibited both TiO_2 (anatase) and copper(II)oxide (monoclinic CuO at $2\theta = 35.7^\circ$ and 38.9° [34,35]) signals. No peak associated to copper(I) oxide was detected, according to the thermal treatment used (calcination at 550 °C) [35,36]. The XRD peaks at about $2\theta = 30^\circ$ were due to residuals of polystyrene spheres. The lack of signals of the $BiVO_4$ and CuO, when their amount was lower than 10 wt.%, was presumably due to the low content and/or high dispersion (small particle size) of the host oxide in I.O. TiO_2 composites.

The average crystallites size of TiO_2 in the investigated composites, determined by applying the Scherrer formula using the (1 0 1) anatase diffraction peak ($2\theta = 25.3^\circ$), is reported in Table 1. In the I.O. TiO_2-$BiVO_4$ system, the TiO_2 crystal size varied slightly and progressively with the amount of bismuth vanadate from ca. 25 to ca. 29 nm. In the I.O. TiO_2-CuO composites, the TiO_2 crystal sizes slightly decreased for low amounts of copper oxide (from ca. 25 to 20 nm). This can be ascribed to the introduction of CuO nanoparticles in the crystal lattice of I.O. TiO_2 (the copper precursor was added together with titanium isopropoxide, before the thermal treatment), thus inhibiting the TiO_2 aggregation [37]. This process was favoured when the amount of copper oxide was low. Consequently, a slight increase of the BET surface area values was detected for the I.O. TiO_2-CuO samples with a CuO amount < 5 wt.% (Table 1), whereas no significant variation was found in the I.O. TiO_2-$BiVO_4$ series. The macroporous structure of the catalysts was further confirmed by the type II N_2 adsorption-desorption isotherms [38] found for all of the investigated samples.

To evaluate the optical properties of the samples, their UV–vis DRS spectra and band gap energies, E_g, determined by the modified

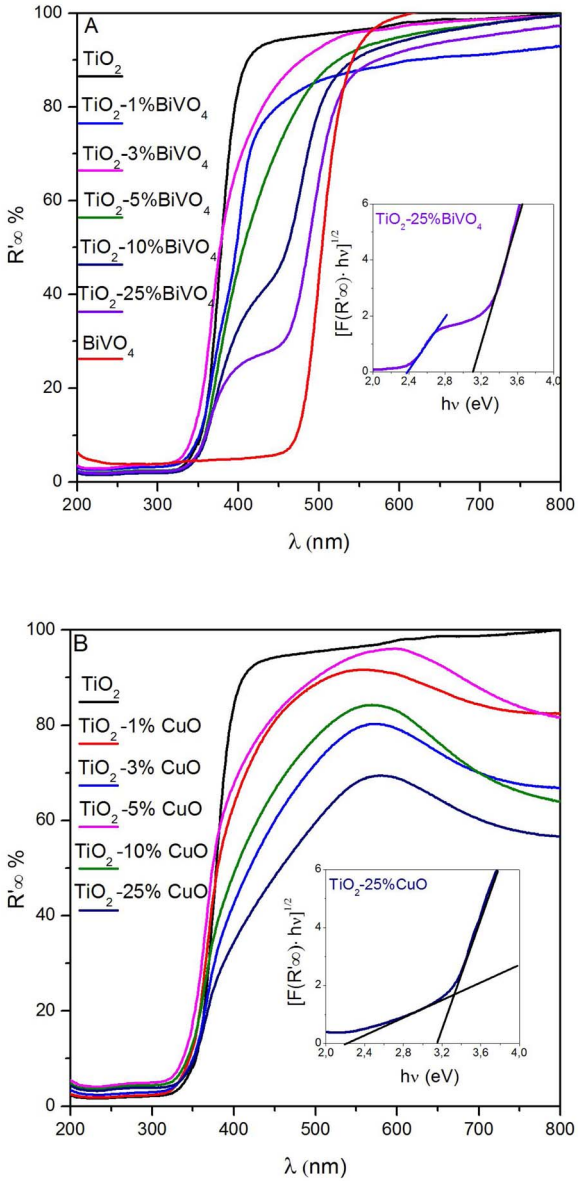

Fig. 5. UV–vis Diffuse reflectance spectra of (A) Inverse Opal TiO_2-$BiVO_4$ and (B) Inverse Opal TiO_2-CuO composites (For interpretation of the references to colour in this figure text, the reader is referred to the web version of this article.)

Kubelka–Munk function, $[F(R_\infty')\ h\nu]^{1/2}$, are reported in Fig. 5 and Table 1 respectively.

The I.O. TiO_2-$BiVO_4$ system (Fig. 5A) showed an enhancement of absorption in the visible region by increasing the amount of bismuth vanadate. Consequently a decrease of the band-gap energy was observed (Table 1). It is noteworthy that another absorption feature at about 400 nm was detected in the samples with higher $BiVO_4$ amounts, more evident for the TiO_2-25%$BiVO_4$ catalyst. As it can be seen in the inset of Fig. 5A, plotting $[F(R_\infty')\ h\nu]^{1/2}$ versus the energy of the exciting light for TiO_2-25%$BiVO_4$, two contributes were found, one at 3.19 eV, due to I.O. TiO_2 and another at 2.40 eV, due to monoclinic $BiVO_4$ [39,40]. In accordance with the literature, the presence of these two features suggests the formation of a heterostructure between the I.O. TiO_2 and the $BiVO_4$ [41].

By increasing the CuO amount, a higher absorption in the visible region (Fig. 5B) which is typical of the presence of Cu species can be noticed [42]. The latter ones create additional energy levels in the band gap of TiO_2 [35,37], as confirmed by the presence of a midgap band located above the valence band in the sample containing high CuO amounts (inset of Fig. 5B). A small decrease (0.05-0.09 eV) of the TiO_2 band-gap energies can be also observed (Table 1). As reported in the literature, CuO electrons can give excitation from the valence band to the exciton level (< 730 nm), d−d transition of Cu^{2+} giving absorption in the 600–800 nm range. Moreover, it has been reported [43] that the presence of Cu(II) causes a shift of the valence band edge towards less positive values, and consequently a decrease of the band gap.

To investigate the oxidation states and the surface composition of involved species, XPS measurements of the I.O. TiO_2 composites were carried out and the results summarized in Table 2.

Regarding the I.O. TiO_2-$BiVO_4$ composites, the signals detected in the vanadium and in the bismuth zone are characteristic of V(V) and Bi (III) [44,45], whereas no substantial shift compared to I.O. TiO_2 was measured in the Ti and O XPS regions. Noteworthy the surface atomic concentrations of V and Bi in the I.O. TiO_2-3%$BiVO_4$ are very low (Table 2). Probably (according to XRD data) the use of a little amount of precursor salts favours the dispersion of $BiVO_4$ at the interface of TiO_2.

The binding energies values of the Cu 2p zone indicate that copper is mostly present on the surface of I.O. TiO_2 as Cu^{2+} [46,47]. In this case, the I.O. TiO_2-25% CuO exhibited 0.6 eV and 1 eV shifts at higher binding energy compared to I.O. TiO_2 both in Ti and O regions, respectively. In accordance with the literature [48] this shift can be ascribed to the electron transfer from TiO_2 to CuO (also in agreement to DRS measurements), favoured at high amounts of copper oxide. In accordance with *Avgouropoulos* et al. [49] both the Cu^{+1} and Cu^{+2} can contribute to the Cu $2p_{3/2}$ peak and these signals are typically in the 932.5-932.8 eV range. Our signals at 933.2 eV for I.O. TiO_2-3%CuO and at 933.9 eV for I.O. TiO_2-25%CuO are consistent with the presence of Cu^{+2}, confirming the XRD data. The signal at 953.0 eV could be tentatively attributed to Cu^0 in accordance with *Wu* et al. [50]. The shapes of the XPS spectra revealed that the copper species on TiO_2 are major CuO and minor Cu^0. By comparing the atomic percentages of Bi^{3+} and Cu^{2+}, it can be seen that $BiVO_4$ is dispersed within the TiO_2 matrix, whilst CuO is mostly present on the surface.

The above reported results indicate that the combination of structural (obtainment of an inverse opal backbone) and chemical (presence $BiVO_4$ or CuO) modifications of TiO_2 is capable of enhancing the

Table 2
XPS binding energies and atomic composition of the investigated I.O. TiO_2 catalysts.

Catalysts	Ti 2p (eV)	O 1s (eV)	V 2p (eV)	Bi 4f (eV)	Cu 2p (eV)	Ti (at%)	O (at%)	Bi (at%)	V (at%)	Cu (at%)
I.O.-TiO_2	458.8 464.8	529.8 531.6	–	–	–	30.5	55.7	–	–	–
TiO_2- 3%$BiVO_4$	458.9 464.9	529.6 532.4	516.0 523.6	low intensity	–	32.8	58.8	0.01	0.04	–
TiO_2- 25%$BiVO_4$	458.5 464.5	530.2 531.2	517.0 524.5	159.5 164.5	–	28.6	51.5	1.7	0.9	–
TiO_2- 3%CuO	458.8 464.8	530.3 531.9	–	–	933.2 953.0	25.3	59.1	–	–	1.2
TiO_2- 25%CuO	459.4 465.4	530.8 532.6	–	–	933.9 953.0	27.6	52.2	–	–	9.9

photocatalytic H_2 production. In particular, the presence of a macroporous structure such as that of I.O. TiO_2 largely improves the absorption of photons, increasing the path length and the migration rate of electron-hole pairs towards the surface. Consequently the reduction of H^+ ions on the surface of TiO_2 by the photogenerated electrons is favoured [29,30]. This well agrees with the observed higher photoactivity of I.O. TiO_2 compared to commercial TiO_2. This photoactivity is further increased in the presence of $BiVO_4$. The sample with the highest $BiVO_4$ content, I.O. TiO_2-25%$BiVO_4$, exhibited the best performance both under UV and solar irradiation. Due to the small band-gap of $BiVO_4$, the produced high-energy electrons in the bare $BiVO_4$ relax easily from the conduction (CB) to the valence band (VB) in a remarkably short period, with obvious energy loss, leading to an inefficient charge separation. The coupling of $BiVO_4$ with TiO_2 leads to an increase of photocatalytic performances. As reported in the literature, in fact, $BiVO_4$ can be considered as a light sensitizer for TiO_2. In particular, a generally accepted mechanism considers that under a suitable light irradiation ($\lambda_{excitation} \leq$ 510–530 nm) the electrons of the valence band of $BiVO_4$ are firstly excited to the conduction band of $BiVO_4$, leaving holes behind, and after that these photogenerated electrons are transferred to the CB of TiO_2 [24,51]. The formation of an efficient heterojunction between TiO_2 and $BiVO_4$ is a key factor to explain the enhanced photoactivity. On the basis of XRD, XPS and DRS measurements we found that the heterojunction was favoured only for high amount of $BiVO_4$ (> 10 wt%). This is in good agreement with the results of Zalfani et al. [25], who investigated the photodegradation of Rhodamine B under visible light irradiation over $BiVO_4$-TiO_2 catalysts.

Fig. 6 depicts the band positions versus the Normal Hydrogen Electrode (NHE) of the different semiconductors according to the literature data [52–56]. In the TiO_2-$BiVO_4$ systems (Fig. 6A), electrons can be transferred from $BiVO_4$ to TiO_2 because the conduction band of $BiVO_4$ is more negative than that of TiO_2, whilst holes, due to the more positive valence band of TiO_2, can move in the opposite direction allowing a very efficient charge separation and an improvement of the photocatalytic activity. On the contrary, in the TiO_2-CuO samples (Fig. 6B), both holes and electrons will transfer and accumulate on CuO, giving rise also to some extent of recombination, because the conduction band of CuO is more positive than that of TiO_2, making consequently the junction not very efficient under UV irradiation. Consequently the bare I.O. TiO_2 sample showed to be more active than the TiO_2-CuO samples. However, from an electrochemical point of view, CuO could favour H_2 formation only if its conduction band edge was more negative than the H^+/H_2 potential. In accord to *Yu* et al. [56], when the CuO amount is not very high (1 and 3 wt%, in this paper), particle size is small and the valence and conduction band edges shift toward more positive and more negative values, respectively. In particular the conduction band edge can become more negative than the H^+/H_2 potential, allowing H_2 evolution. This finding could explain the highest activity of the I.O. TiO_2-1%CuO and I.O. TiO_2-3%CuO samples with respect to the other composites samples. In addition, some authors [35,52,53] explain the CuO efficiency toward H_2 production by considering that electron excess on CuO under irradiation causes a negative shift of the Fermi level of the oxide, enabling H^+ reduction.

It is worth noting that according to literature [57–59], H_2 formation can derive both from H_2O splitting and ethanol reforming, while the presence of CO_2 detected during the photocatalytic tests can be related to the mineralization of the organic compound acting as a sacrificial agent.

Contrarily to what observed under UV irradiation, I.O.TiO_2-CuO composites with the smallest amounts of CuO (< 5 wt.%) show to be more photoactive under solar light irradiation with respect to I.O. TiO_2. It is not easy to explain this apparent contradictory behaviour. A tentative explanation can be provided by considering (i) that only a smaller fraction of efficient UV photons are present in the 300 W lamp simulating solar light (with respect to the high number of photons deriving from the 100 W UV lamp) which could give rise to a levelling

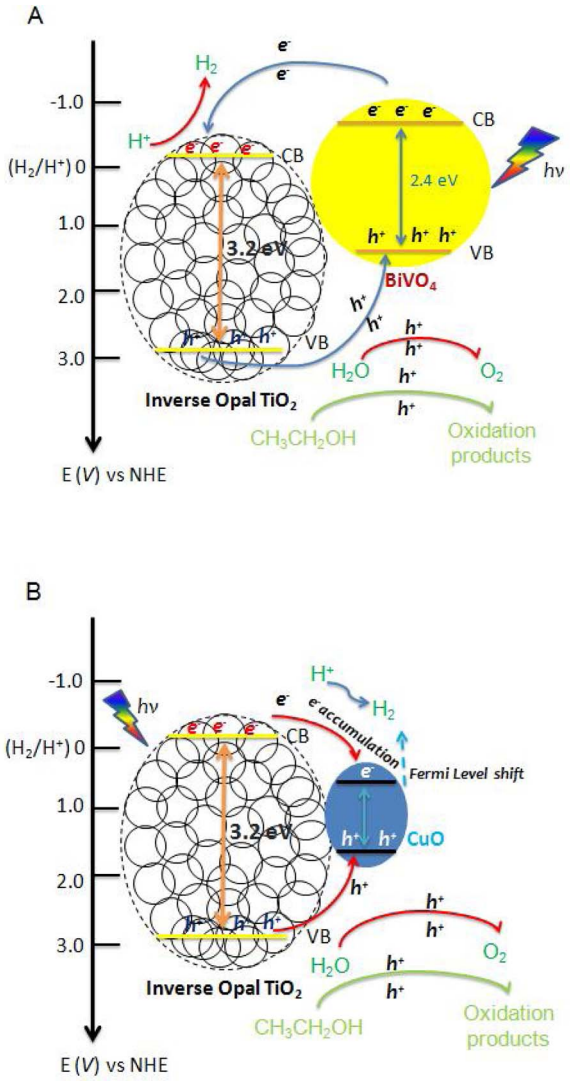

Fig. 6. Possible photocatalytic mechanism of H_2 generation over (A) Inverse Opal TiO_2-$BiVO_4$ and (B) Inverse Opal TiO_2-CuO composites.

effect in the accumulation/recombination of pairs, (ii) that a beneficial effect could be due to the presence of CuO which absorbs in the visible range with the occurrence of d-d transition in Cu^{2+} species (as detected by DRS measurements), thus favouring the accumulation of electrons in the CB of the oxide [42,53].

XRD and DRS results suggest that the incorporation of small amounts of CuO in the inverse opal TiO_2 allows the occurrence of a charge tunneling through the interface barrier between the two oxides. CuO could act as a co-catalyst, offering the reduction sites for H_2 production (Fig. 6B). The presence of a high CuO loading appears to be detrimental as the oxide acts as a recombination site between the charge carriers and the band position is unfavorable due to the particle size increase. Moreover, the lower performance of the systems with high amount of CuO can be due to the lack of activity of CuO and to the segregation of copper oxide on the TiO_2 surface (see XPS results) that hinders light absorption by TiO_2 [60,61].

4. Conclusions

Inverse opal TiO_2-$BiVO_4$ and TiO_2-CuO samples have been synthesized, characterized and tested in the photocatalytic water splitting under both UV and solar light irradiation. The influence of the addition of different amounts of $BiVO_4$ and CuO was evaluated both in terms of

chemico-physical properties and photocatalytic activity.

The peculiar porous backbone of inverse opal TiO_2 increases the path length of the light inside the materials leading to a high light absorption and enhancing the migration rate of electron-hole pairs towards the surface, thus resulting in a higher activity compared to the commercial TiO_2 both under UV and solar light irradiation. A further improvement in terms of H_2 production was also verified by addition of an increasing amount of $BiVO_4$. On the contrary, for the I.O. TiO_2-CuO composites, small copper oxide content was found to be optimal. In fact, due to surface segregation of copper, a higher amount of CuO can decrease the absorption of photon energy on TiO_2 surface due to the coverage of the TiO_2 active sites.

Combination of TiO_2 structural modifications as the synthesis of inverse opal materials, and chemical modifications as the addition of a host $BiVO_4$ or CuO can be a promising strategy to enhance the H_2 production by photocatalytic water splitting.

Acknowledgments

We thank Prof. Bao-Lian Su, director of Laboratory of Inorganic Materials Chemistry (CMI), University of Namur (Belgium), for the materials characterization facilities.

References

[1] D.Y.C. Leung, X. Fu, C. Wang, M. Ni, M.K.H. Leung, X. Wang, X. Fu, ChemSusChem 3 (2010) 68.
[2] X. Chen, S. Shen, L. Guo, S.S. Mao, Chem. Rev. 110 (2010) 6503.
[3] A. Fujishima, K. Honda, Nature 238 (1972) 37.
[4] V. Augugliaro, M. Bellardita, V. Loddo, G. Palmisano, L. Palmisano, S. Yurdak, J. Photochem. Photobiol. C 13 (2012) 224.
[5] M. Ni, M.K.H. Leung, D.Y.C. Leung, K. Sumathy, Renew. Sustain. Energy Rev. 11 (2007) 401.
[6] J.H. Pan, X. Zhao, W.I. Lee, Chem. Eng. J. 170 (2011) 363.
[7] Y. Ye, C. Jo, I. Jeong, J. Lee, Nanoscale 5 (2013) 4584.
[8] L. Xin, X. Liu, RSC Adv. 5 (2015) 71547.
[9] M. Wu, J. Liu, J. Jin, C. Wang, S. Huang, Z. Deng, B.L. Su, Appl. Catal. B: Environ. 150–151 (2014) 411.
[10] J. Ginter, A. Kisielewska, K. Spilarewicz-Stanek, M. Cichomski, D. Batory, I. Piwonsk, Microporous Mesoporous Mater. 225 (2016) 580.
[11] F. Sordello, V. Maurino, C. Minero, J. Mater. Chem. 21 (2011) 19144.
[12] G. Liao, S. Chen, X. Quan, H. Chen, Y. Zhang, Environ. Sci. Technol. 44 (2010) 3481.
[13] A. Kudo, Y. Miseki, Chem. Soc. Rev. 38 (2009) 253.
[14] M. Bellardita, E.I. García-López, G. Marcì, L. Palmisano, Int. J. Hydrogen Energy 41 (2016) 5934.
[15] R. Fiorenza, M. Bellardita, L. D'Urso, G. Compagnini, L. Palmisano, S. Scirè, Catalysts 6 (2016) 121.
[16] Z. Yan, H. Wu, A. Han, X. Yu, P. Du, Int. J. Hydrogen Energy 39 (2014) 13353.
[17] S.J.A. Moniz, J. Tang, ChemCatChem 7 (2015) 1659.
[18] V. Gombac, L. Sordelli, T. Montini, J.J. Delgado, A. Adamski, G. Adami, M. Cargnello, S. Bernal, P. Fornasiero, J. Phys. Chem. A 114 (2010) 3916.
[19] Z. Wang, Y. Liu, D.J. Martin, W. Wang, J. Tang, W. Huang, Phys. Chem. Chem. Phys. 15 (2013) 14956.
[20] G. Li, N.M. Dimitrijevic, L. Chen, T. Rajh, K.A. Gray, J. Phys. Chem. C 112 (2008) 19040.
[21] Z. He, Y. Shi, C. Gao, L. Wen, J. Chen, S. Song, J. Phys. Chem. C 118 (2014) 389.
[22] T.W. Kim, K.S. Choi, Science 343 (2014) 990.
[23] Z. Jian, S. Huang, Y. Cao, Y. Zhang, Photochem. Photobiol. 92 (2016) 363.
[24] M. Xie, X. Fu, L. Jing, P. Luan, Y. Feng, H. Fu, Adv. Energy Mater. 4 (2014) 1300995.
[25] M. Zalfani, Z.Y. Hu, W. Yu, M. Mahdouani, R. Bourguiga, M. Wu, Y. Li, B. van, G. Van Tendeloo, Y. Djaoued, B.L. Su, Appl. Catal. B Environ. 205 (2017) 121.
[26] Y. Guo, X. Yang, F. Ma, K. Li, L. Xu, X. Yuan, Y. Guo, Appl. Surf. Sci. 256 (2010) 2215.
[27] C. Su, B.Y. Hong, C.M. Tseng, Catal. Today 96 (2004) 119.
[28] G. Marcì, V. Augugliaro, M.J. López-Muñoz, C. Martín, L. Palmisano, V. Rives, M. Schiavello, R.J.D. Tilley, A.M. Venezia, J. Phys. Chem. B 105 (2001) 1026.
[29] H. Xu, X. Chen, S.X. Ouyang, T. Kako, J.H. Ye, J. Phys. Chem. C 116 (2012) 3833.
[30] J.I.L. Chen, E. Loso, N. Ebrahim, G.A. Ozin, J. Am. Chem. Soc. 130 (2008) 5420.
[31] S. Konar, H. Kalita, N. Puvvada, S. Tantubay, M. Kr Mahto, S. Biswas, A. Pathak, J. Catal. 336 (2016) 11.
[32] A.K. Bhattacharya, K.K. Mallick, A. Hartridge, Mater. Lett. 30 (1997) 7.
[33] C.M. Huang, G.T. Pan, P.Y. Peng, T.C.K. Yang, J. Mol. Catal. A: Chem. 327 (2010) 38.
[34] J.F. Xu, W. Ji, Z.X. Shen, S.H. Tang, X.R. Ye, D.Z. Jia, X.Q. Xin, J. Solid State Chem. 147 (199) (2016) 516.
[35] J. Bandara, C.P.K. Udawatta, C.S.K. Rajapakse, Photochem. Photobiol. Sci. 4 (2005) 857.
[36] Z.N. Kayani, M. Umer, S. Riaz, S. Naseem, J. Electron. Mater. 44 (2015) 3704.
[37] R. Yang, L. Yang, T. Tao, F. Ma, M. Xu, Z. Zhang, Appl. Surf. Sci. 288 (2014) 363.
[38] H. Yan, C.F. Blanford, B.T. Holland, W.H. Smyrl, A. Stein, Chem. Mater. 12 (2000) 1134.
[39] A. Kudo, K. Omori, H. Kato, J. Am. Chem. Soc. 121 (1999) 11459.
[40] Y. Hu, D. Li, Y. Zheng, W. Chen, Y. He, Y. Shao, X. Fu, G. Xiao, Appl. Catal. B 104 (2011) 30.
[41] S. Obregón, G. Colón, RSC Adv. 4 (2014) 6920.
[42] M. Bellardita, A. Di Paola, E. García-López, V. Loddo, G. Marcì, L. Palmisano, Curr. Org. Chem. 17 (2013) 2440.
[43] A. Di Paola, E. García-López, G. Marcì, C. Martín, L. Palmisano, V. Rives, A.M. Venezia, Appl. Catal. B 48 (2004) 223.
[44] N. Myung, S. Ham, S. Choi, Y. Chae, W. Kim, Y.J. Jeon, K. Paeng, W. Chanmanee, N.R. de Tacconi, K. Rajeshwar, J. Phys. Chem. C 115 (2011) 7793.
[45] L. Dong, S. Guo, S. Zhu, D. Xu, L. Zhang, M. Huo, X. Yang, Catal. Commun. 16 (2011) 250.
[46] H. Yu, H. Irie, K. Hashimoto, J. Am. Chem. Soc. 132 (2010) 6898.
[47] H. Irie, K. Kamiya, T. Shibanuma, S. Miura, D.A. Tryk, T. Yokoyama, K. Hashimoto, J. Chem. Phys. C 113 (2009) 10761.
[48] B.F. Xin, P. Wang, D.D. Ding, J. Liu, Z.Y. Ren, H.G. Fu, Appl. Surf. Sci. 254 (2008) 2569.
[49] G. Avgouropoulos, T. Ioannides, Appl. Catal. A 244 (2003) 155.
[50] J.C.S. Wu, I.H. Tseng, W.C. Chang, J. Nanopart. Res. 3 (2001) 113.
[51] J. Sun, X. Li, Q. Zhao, M.O. Tadé, S. Liu, J. Mater. Chem. A 3 (2015) 21655.
[52] H. Hou, M. Shang, F. Gao, L. Wang, Q. Liu, J. Zheng, Z. Yang, W. Yang, ACS Appl. Mater. Interfaces 8 (2016) 20128.
[53] S. Xu, J. Ng, A.J. Du, J. Liu, D.D. Sun, Int. J. Hydrogen Energy 36 (2011) 6538.
[54] S. Moniz, S.A. Shevlin, D. Martin, Z. Guo, J. Tang, Energy Environ. Sci. 8 (2015) 731.
[55] J. Resasco, H. Zhang, N. Kornienko, N. Becknell, H. Lee, J. Guo, A.L. Briseno, P. Yang, ACS Cent. Sci. 2 (2016) 80.
[56] J. Yu, Y. Hai, M. Jaroniec, J. Colloid Interface Sci. 357 (2011) 223.
[57] A. Patsoura, D.I. Kondarides, X.E. Verykios, Catal. Today 124 (2007) 94.
[58] C.R. López, E. Pulido Melián, J.A. Ortega Méndez, D.E. Santiago, J.M. Doña Rodríguez, O. González Díaz, J. Photochem. Photobiol. A 312 (2015) 45.
[59] T. Puangpetch, T. Sreethawong, S. Yoshikawa, S. Chavadej, J. Mol. Catal. A: Chem. 312 (2009) 97.
[60] S. Xu, D.D. Sun, Int. J. Hydrogen Energy 34 (2009) 6096.
[61] L. Delannoy, G. Thrimurthulu, P.S. Reddy, C. Méthivier, J. Nelayah, B.M. Reddy, C. Ricolleaudand, C. Louisa, Phys. Chem. Chem. Phys. 16 (2014) 26514.